J. Fluid Mech. (1997), *vol.* 343, *pp.* 1–28. Printed in the United Kingdom

© 1997 Cambridge University Press

Experimental study of magnetohydrodynamic flows in electrically coupled bends

By R. STIEGLITZ[1] AND S. MOLOKOV[2]

[1] Institute for Applied Thermo- and Fluiddynamics (IATF), Forschungszentrum Karlsruhe GmbH, Postfach 3640, D-76021 Karlsruhe, Germany

[2] Coventry University, School of Mathematical and Information Sciences, Priory Street, Coventry CV1 5FB, UK

(Received 22 May 1996 and in revised form 6 January 1997)

An experimental study of a magnetohydrodynamic flow in a system of n ($n \leqslant 5$) U-bends is presented. The bends are electrically coupled via common electrically conducting walls parallel to the external magnetic field. In the test section the fluid flows perpendicular–parallel–perpendicular to the magnetic field. The Hartmann number M varies in the range $6 \times 10^2 \leqslant M \leqslant 2.4 \times 10^3$, and the interaction parameter N in the range $10^2 \leqslant N \leqslant 4.3 \times 10^4$. The experimental data for the wall electric potentials and the pressure have been compared with the theoretical asymptotic values calculated for $N \gg M^{3/2} \gg 1$. This assumption in theory ensures the inertialess nature of the flow. For $n = 1$ the agreement between the theory and the experiment is good. With increasing number of bends quantitative (for $n = 3$) and then qualitative (for $n = 5$) disagreement appears. For the first time in strong-field magnetohydrodynamics this disagreement has been observed on the Hartmann walls, i.e. walls perpendicular to the field. The experimental results for the wall potential indicate that for $n = 5$ in some of the ducts parallel to the field qualitatively different flow patterns are established than those predicted by the asymptotic inertialess theory. The flow in the core depends on N, i.e. is of inertial nature. In the whole range of N investigated there is only a slight tendency of the wall potential to approach theoretical values. This demonstrates the stability of the new flow pattern and that even such high values of N as 4.3×10^4 are insufficient for the core flow to be inertialess. A strong dependence of the pressure drop on N has been observed in all the flow configurations investigated. The dependence of the inertial part of the pressure drop in each bend scales with $N^{-1/3}$, as long as $N^{-1/3} \ll 1$. This is characteristic of electromagnetic–inertia interaction in the boundary and internal layers parallel to the field. A linear increase of the pressure drop with the number of coupled bends has been observed, confirming qualitatively previous theoretical results. The effects of magnetic field inclination and different flow distribution between bends have also been studied.

1. Introduction

In the fusion blanket application of magnetohydrodynamics (MHD) (Malang *et al.* 1988) a liquid metal flows in a very strong magnetic field, so that both the Hartmann number $M = aB_0(\sigma/(\rho\nu))^{1/2}$ and the interaction parameter $N = a\sigma B_0^2/(\rho v_0)$ are high, in the range 10^2–10^5. The interaction parameter and the square of the Hartmann number express the ratios of electromagnetic to inertia and viscous forces, respectively. In the above σ, ν and ρ are the electrical conductivity, kinematic viscosity and density of the fluid, B_0 is the induction of the uniform applied magnetic field, v_0 is the average fluid

https://doi.org/10.1017/S0022112097005788 Published online by Cambridge University Press

velocity, and a is a characteristic duct dimension. At such extreme values of parameters M and N the MHD flows in rectangular ducts are usually modelled with the use of asymptotic methods for $N \gg M^{3/2} \gg 1$, since direct methods of numerical integration fail. The assumption $N \gg M^{3/2} \gg 1$ ensures that inertia effects are negligible in the whole flow region, while viscous effects are confined to thin boundary and internal layers, where the flow is governed by *viscous–electromagnetic* interaction. In the experiments with straight rectangular ducts in a smoothly varying magnetic field in the direction of the flow (Reed *et al.* 1987) a very good agreement with the theoretical results for the inertialess flow has been achieved. The agreement was good despite the fact that the assumption $N \gg M^{3/2}$, which was very difficult if not impossible to fulfil in the experiments, did not hold. In fact in these experiments the values of N were $N \approx M^{3/2}$ and even $N \ll M^{3/2}$. First, experiments with bends in the plane of the field (Barleon *et al.* 1993, 1994) also showed quite good agreement with the asymptotic theory. These facts gave a rise to the expectation that general three-dimensional flows in strong magnetic fields may be described on the basis of the inertialess flow model even for $N < M^{3/2}$.

However, recently Reimann *et al.* (1993, 1995) and Stieglitz *et al.* (1996) presented experimental evidence that in complex elements such as rectangular bends in the plane of the field both the pressure drop and the flow pattern may be different, sometimes qualitatively different from the asymptotic ones obtained in the inertialess limit.

Reimann *et al.* (1993) performed screening experiments with a system of electrically coupled U-bends and found that the pressure drop strongly depends on the interaction parameter, showing the importance of inertia effects neglected in the model. Later Reimann *et al.* (1995) performed experiments with a single U-bend. They used hot-wire and electromagnetic probes to measure velocity profiles and potential gradients within the liquid metal in two sets of measurements. At the relatively low values of $N \leqslant 150$ and $M \leqslant 460$ they discovered unexpected velocity profiles to be discussed in §5. The tendencies were opposite to those in the model. In particular, the vorticity component in the magnetic field direction was of the opposite sign.

Stieglitz *et al.* (1996) presented measurements of the wall potential, pressure and potential gradient within the liquid metal in a Z-shaped bend. No qualitative difference with the theory was discovered in the electric potential on the Hartmann walls (walls with significant normal component of the magnetic field). However, both the pressure drop and the sidewall (walls parallel to the field) potential showed the dependence on N as $N^{-1/3}$, which is characteristic of *electromagnetic–inertia* interaction in the boundary and internal layers. This is a completely different type of force balance than in the asymptotic model discussed above and developed for bend flows by Moon & Walker (1990), Moon, Hua & Walker (1991), Hua & Walker (1991), Bühler (1993, 1995), Molokov & Bühler (1994, 1995) and Molokov & Stieglitz (1995). This difference was discussed by Hunt & Leibovich (1967), Hunt & Holroyd (1977), and recently by Molokov, Bühler & Stieglitz (1995). Measurements of the potential gradient within the liquid metal showed both quantitative (up to 400 %) and qualitative differences with the theory.

It should be noted that measurements of the potential gradient and the fluid velocity within the liquid metal in essentially three-dimensional flows may be not precise because of the well-known negative influence of the probe on the flow pattern (see the discussion by Stieglitz *et al.* 1996). For example, Reimann *et al.* (1995) report a difference of almost 100 % in some readings by the two different measurement techniques (see above). Therefore, a more convincing confirmation of their results is necessary.

https://doi.org/10.1017/S0022112097005788 Published online by Cambridge University Press

Measurement of the wall potential is much more precise, since the probe tips attached to the outside wall surface produce a negligible influence on the flow. In this paper the results of such measurements are presented for a system of n electrically coupled U-bends for $n = 1, 3$ and 5. We show that for $n = 5$ a qualitatively different *wall potential distribution* is established in ducts parallel to the magnetic field than that predicted by the theory. This distribution obtained on the Hartmann walls indirectly indicates that the flow pattern must also be qualitatively different (see §5). No significant difference with the theory has been observed for $n = 1$, while for $n = 3$ the difference is significant but only quantitative.

Another aspect of the flow in a system of bends studied here experimentally is the electromagnetic flow coupling resulting from circulation of global electric currents. A comparison between the experiment and the inertialess theory developed previously (Molokov & Stieglitz 1995) is given. In particular, the effect of increasing the number of bends on the pressure drop in inertial MHD flows is studied. This question is of paramount importance for the fusion blanket technology. However, concerning both the pressure drop and the flow pattern we discuss main tendencies of general interest, while technical results of importance to fusion blanket designers only are discussed elsewhere (Stieglitz 1994 and Stieglitz *et al.* 1994).

2. Formulation

The geometry of the system of bends under consideration is shown in figure 1. It consists of five bends, which are electrically coupled via electrically conducting common walls. The externally applied strong uniform magnetic field $\boldsymbol{B}$ is oriented so that the fluid flows perpendicular–parallel–perpendicular to $\boldsymbol{B}$ in the part of the test section investigated, the so-called U-bends. To keep to the terminology commonly used in fusion design, the fluid flows in radial–toroidal–radial U-bends. All ducts have square cross-sections in each part of the bend. The whole geometry is symmetric with respect to the midplane of the central duct $i = 1$ (symmetry plane S1, $z = 0$). The part of the test section under investigation, i.e. radial–toroidal–radial U-bend, is also symmetric with respect to the plane S2 at $y = l$. Contrary to the analysis performed by Molokov & Stieglitz (1995) the radial ducts are of finite length, namely l_{rad}, and they are fed by the supplying ducts, which are parallel or almost parallel to the field. Part of the supplying ducts for $y < -4$ are turned by an angle of 7°, so that the test section as a whole is slightly asymmetric with respect to S2. The definition of the other length scales may be taken from figure 1.

The steady flow of an electrically conducting viscous incompressible fluid in bend i of the system of bends is governed by the following dimensionless inductionless MHD equations:

momentum
$$\frac{1}{N}\left[\frac{\partial \boldsymbol{v}^{(i)}}{\partial t} + (\boldsymbol{v}^{(i)} \cdot \boldsymbol{\nabla})\, \boldsymbol{v}^{(i)}\right] = -\boldsymbol{\nabla} p^{(i)} + \frac{1}{M^2}\Delta \boldsymbol{v}^{(i)} + \boldsymbol{j}^{(i)} \times \boldsymbol{B}, \tag{2.1}$$

mass
$$\boldsymbol{\nabla} \cdot \boldsymbol{v}^{(i)} = 0, \tag{2.2}$$

charge
$$\boldsymbol{\nabla} \cdot \boldsymbol{j}^{(i)} = 0, \tag{2.3}$$

and Ohm's law
$$\boldsymbol{j}^{(i)} = -\boldsymbol{\nabla} \Phi^{(i)} + \boldsymbol{v}^{(i)} \times \boldsymbol{B}. \tag{2.4}$$

The velocity $\boldsymbol{v}$, the magnetic field $\boldsymbol{B}$, the current density $\boldsymbol{j}$, the pressure p, the potential Φ, and time t are normalized by the average fluid velocity v_0 in the whole system of

https://doi.org/10.1017/S0022112097005788 Published online by Cambridge University Press

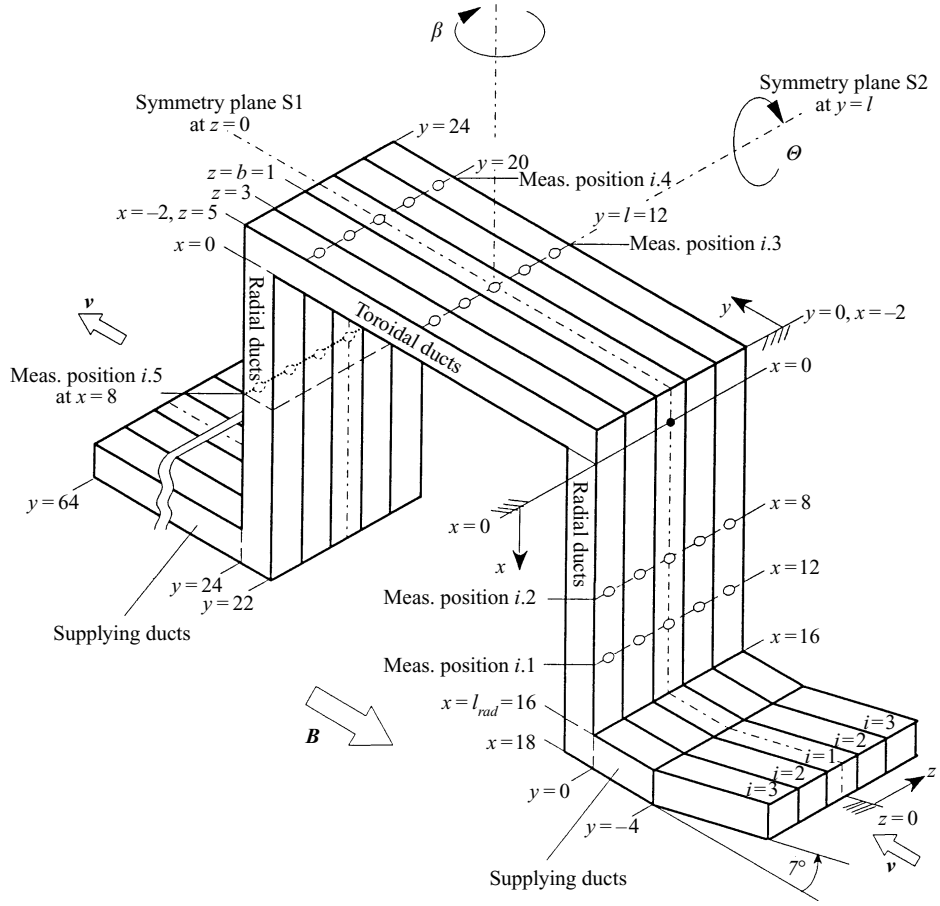


FIGURE 1. Schematic of the test section. The locations of the measurement positions for pressure are shown with circles.

bends, B_0, $\sigma v_0 B_0$, $a\sigma v_0 B_0^2$, $a v_0 B_0$, and a/v_0, respectively. The length scale a represents half the height of the radial ducts in the magnetic field direction; all other length scales appearing in the problem are normalized by a. The fluid properties are assumed to be constant. Equations (2.1)–(2.4) are based on the assumption that the induced magnetic field arising from the electric current flow within the fluid and in the duct walls is negligibly small, so that the applied magnetic field can be considered as constant.

The boundary condition for the fluid velocity at each wall is the no-slip condition

$$\boldsymbol{v}^{(i)}|_W = 0. \tag{2.5}$$

The electric boundary condition at the duct walls facing the environment is the thin-wall condition

$$(\boldsymbol{j}\cdot\boldsymbol{n})^{(i)} = -c\Delta_\tau \Phi_W^{(i)}, \tag{2.6}$$

see Walker (1981), where $\Phi_W^{(i)}$ is the potential of the duct wall, $\boldsymbol{n}^{(i)}$ is the inward normal unit vector to the wall, Δ_τ is the two-dimensional Laplace operator in the plane of the wall, $c = t_W \sigma_W/(a\sigma)$ is the wall conductance ratio, t_W and σ_W are the thickness and the electrical conductivity of the wall. The wall conductance ratio c expresses the ratio of the electrical conductance of the wall to that of the fluid, and is the same for all walls

https://doi.org/10.1017/S0022112097005788 Published online by Cambridge University Press

of the test section. Condition (2.6) has to be modified at the interior dividing walls common to ducts i and $i+1$ to give

$$(\boldsymbol{j}\cdot\boldsymbol{n})^{(i+1)}+(\boldsymbol{j}\cdot\boldsymbol{n})^{(i)}=-c\Delta_{\tau}\Phi_{W}^{(i)}, \tag{2.7}$$

see Hua & Picologlou (1991) and Molokov & Stieglitz (1995). Conditions (2.6) and (2.7) mean that the net current input to the wall from the fluid is balanced by a tangential current flow in the wall, creating a potential distribution $\Phi_{W}^{(i)}$.

Finally, the potential at the fluid–wall interface is continuous, i.e.

$$\Phi_{Fluid}^{(i)}|_{W}=\Phi^{(i)}|_{W}, \tag{2.8}$$

if no electric contact resistance at the interface exists. Many structural materials, e.g. stainless steel, have a passivated surface in the form of oxides or alloys arising from the manufacturing process and therefore have an undefined electrical contact. The contact resistance is removed before the experiment by the so-called wetting procedure (see Stieglitz *et al*. 1996). The effect of the contact resistance on the velocity profiles and the pressure drop may be dramatic, see Bühler & Molokov (1994).

3. Analysis

A detailed asymptotic analysis of the flow in a system of U-bends with semi-infinite radial ducts has been performed by Molokov & Stieglitz (1995). Their analysis is valid for $N\gg M^{3/2}\gg 1$ and $c\gg M^{-1/2}$, or for $M^{3/2}\gg N\gg 1$ and $c\gg N^{-1/3}$. We summarize their results here and discuss modifications to their model dictated by the finite length of the radial ducts in the test section.

At high M viscous effects can be neglected in the momentum balance (2.1) except for the boundary and internal layers. At high N inertia effects may also be neglected. With $N\gg 1$ and $M\gg 1$ the momentum equation reduces to a balance between pressure and Lorentz forces in the cores of the ducts, the pressure being constant along magnetic field lines.

The inviscid cores are separated from the walls and from each other by thin viscous layers. The most important of them are: (i) Hartmann layers at walls normal to the magnetic field; (ii) parallel layers at walls parallel to the magnetic field (the so-called side layers) and at abrupt changes of the geometry in the magnetic field direction (internal layers, such as those at $x=0$). The thickness of the Hartmann layers is $\delta_{H}\sim M^{-1}$. The thickness of the parallel layers depends on the type of force balance there. For $N\gg M^{3/2}$ the inertial effects are negligible, and the flow in the parallel layers is determined by the viscous–electromagnetic interaction, while the thickness of the layer is $\delta_{P}\sim M^{-1/2}$. For $N\ll M^{3/2}$ inertial effects become significant; these layers become thicker with $\delta_{P}\sim N^{-1/3}$, which is determined by electromagnetic–inertia interaction (see Hunt & Leibovich 1967; Hunt & Holroyd 1977; Molokov *et al*. 1995). In the parallel layers high-velocity jets may appear, as shown by Hunt (1965) (see also Walker 1981). These jets may carry a significant part of the volume flux, if not all, and thus play an important role in the overall flow balance.

Simultaneously with the partial differential equations for the boundary layers and the core the partial differential equations for the electric potential on the walls are solved, which result from the boundary conditions (2.6) and (2.7). The potential distribution on the wall is determined by the electric current leaving the fluid domain and entering the wall. If the electrical conductance of the walls is much higher than that of the neighbouring parallel layers ($c\gg\delta_{P}$), most of the core current flows across the parallel layer into the wall without significant changes. The current in the parallel

https://doi.org/10.1017/S0022112097005788 Published online by Cambridge University Press

layers may then be neglected and the differential equation for the wall potential is directly matched to the core flow. The assumption $c \gg \delta_P$ has been used in all the theoretical investigations cited in §1, as well as in the present study. In this case the nature of the parallel layer, whether it is governed by viscous–electromagnetic or electromagnetic–inertia interaction, is unimportant. The parallel layers then play a passive role, and the flow in the layers may be reconstructed, if necessary, after the solution of the problem for the core pressure and the wall potential has been obtained. The latter problem involves two-dimensional equations only (see Molokov & Stieglitz 1995).

Owing to these assumptions of inductionless and inertialess flow, the calculation can be restricted to one half of the U-bend ($y < l$). The effect of the inclination of the supplying ducts for $y < -4$ is expected to be small in the major part of the U-bend. Therefore, at $y = l$ the following symmetry conditions are used:

$$p^{(i)}(y = l) = 0; \quad \Phi^{(i)}(y = l) = 0. \tag{3.1}$$

Fully developed flow conditions cannot be applied in the radial ducts, as in the calculations of Molokov & Stieglitz (1995), since these ducts are of finite length and are fed by the supplying ducts. Instead, the computational domain is extended up to $x = l_{rad}$ with appropriate symmetry conditions between $x = 0$ and $x = l_{rad}$, as has been done by Stieglitz *et al.* (1996) for a Z-bend. For the potentials these conditions are

$$\Phi^{(i)}(l_{rad}, y, z) = \Phi^{(i)}(0, 2a - y, z). \tag{3.2}$$

Owing to symmetry with respect to the plane S1, computational effort can be reduced by introducing the conditions

$$\frac{\partial p^{(1)}}{\partial z}(z = 0) = \Phi^{(1)}(z = 0) = 0 \quad \text{at} \quad z = 0, \tag{3.3}$$

and restricting attention to the region $z \geqslant 0$.

The test section consists of five ducts, which are filled in turn in order to investigate flow in one, then three, and finally five bends. Where flow in less than five bends is investigated the outer ducts remain empty. Their walls, however, serve as an additional path for the electric currents induced in the filled ducts. This current path has been taken into account by solving the Laplace equation

$$\Delta_\tau \Phi_W^{(i)} = 0 \tag{3.4}$$

for the potentials on all walls of non-filled ducts.

The iterative numerical scheme to solve the problem for the wall potentials and the core pressures, together with the boundary and symmetry conditions discussed here, is analogous to that of Molokov & Stieglitz (1995). The resolution of the grid is 16 points per unit length and the iteration process in the calculations is stopped when the relative error in all flow quantities falls below 0.5%.

The main features of the flow in the *toroidal ducts* are the following. In the cores of these ducts the flow velocity is

$$\boldsymbol{v}_{tor,core}^{(i)} = (1 - y/l)\,\hat{\boldsymbol{y}} \times \boldsymbol{\nabla}_{xz} \Phi_W^{(i)}(y = 0) \quad \text{for} \quad -2 < x < 0, \tag{3.5}$$

i.e. the y component of the core velocity vanishes. This implies that the flow in the y-direction is carried in the parallel layers. However, the other two components of the core velocity are non-zero. Thus, the fluid flows in the planes $y =$ constant following the isolines of the potential $\Phi_W^{(i)}(y = 0)$. The projection of the flow pattern on the (x,

https://doi.org/10.1017/S0022112097005788 Published online by Cambridge University Press

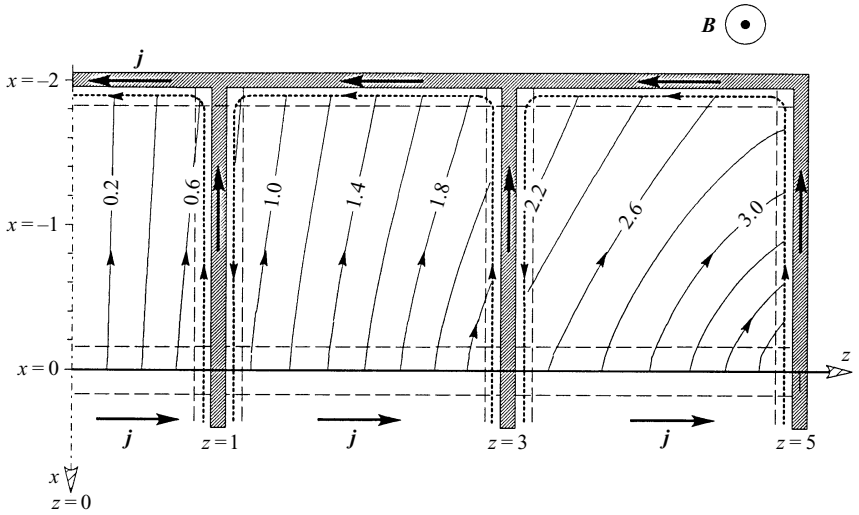


FIGURE 2. Calculated streamlines in the cores of the toroidal ducts (solid lines) for $n = 5$, $Q^{(i)} = \text{constant}$, $c = 0.038$ and $\Theta = \beta = 0°$. They are isopotential lines at the wall $y = 0$; $x \leqslant 0$. The direction of the flow in the parallel layers for $y < 2$ is shown by arrows on dotted lines.

z)-plane for $n = 5$ is shown in figure 2, which demonstrates how flow redistribution between different parallel layers occurs through the core. This redistribution is more intensive at $y = 0$, decreasing linearly to zero at the symmetry plane $y = l$, according to (3.5).

For $y < 2$ there is a volume flux from the right-hand parallel layers of the radial ducts in each bend into the toroidal ducts, which persists over some distance in the toroidal ducts, as shown in figure 2 (dotted lines). Simultaneously, this flow turns in the y-direction to be carried in the parallel layers in the toroidal ducts. For $y > 2$ the tendency reverses so that the projection of the flow direction in the layer on the (x, z)-plane becomes opposite to that in figure 2.

Molokov & Stieglitz (1995) showed that the jets at the two sides of the dividing walls are equal in magnitude but opposite in direction. This means that in the left-hand-side layers in ducts 2 and 3 negative jets appear whenever jets are positive on the opposite side of the dividing walls. For equal flow rates $Q^{(i)} = \text{constant}$ this happens in the whole U-bend, i.e. in both radial and toroidal ducts.

The other important flow properties in the toroidal duct are that the core currents flow only in the magnetic field direction and that there is no pressure drop in the toroidal ducts to the main order. Concerning the pressure drop, the main difference with the flow considered by Molokov & Stieglitz (1995) is that for $n \geqslant 3$ the flow turns out to be not fully developed in the whole test section, as will be discussed in §5.

4. Experimental set-up

The experiments in the multi-channel U-bend test section have been carried out in the MEKKA-facility of the Forschungszentrum Karlsruhe in a super-conducting magnet with a maximum field strength of 3.6 Tesla and a gap of 400 mm. The homogeneous axial field strength, defined as the region in which the magnetic field deviates by less than 10%, is 450 mm long. The liquid metal used in the experiment is the eutectic sodium–potassium alloy $Na^{22}K^{78}$. The thermophysical data of the fluid

https://doi.org/10.1017/S0022112097005788 Published online by Cambridge University Press

may be taken from O'Donell, Papanicolaou & Reed (1989). A detailed description of the experimental facility and the magnet is given by Barleon, Casal & Lenhart (1991), see also Stieglitz *et al.* (1996).

The test section consists of five neighbouring ducts, in which each part of the U-bend has a square cross-section. The characteristic length is $a = 12.5$ mm, which provides the wall conductance ratio of $c = 0.038$. The walls are made of 1 mm thick stainless steel plates. The supplying ducts are formed by ducts aligned with the magnetic field. At the inlet, however, after four values of the characteristic length the ducts are inclined by an angle of 7°, which allows the test section in the (x, y)-plane to be inclined by an angle Θ of up to 7° within the restricted length of the homogeneous field, see figure 1. An inclination of $\beta = 9°$ in the (x, z)-plane has also been investigated. The measurement of the potentials on the duct surface has been carried out using 225 spring loaded needles mounted on a fibreglass matrix which is attached to the test section. The needles are in electrical contact with the duct walls. The probes are arranged in 17 measurement lines in three different planes from $-5 \leqslant z \leqslant 5$ in the following way: plane $y = 0$ at $x = -1, 0, 2, 4, 6$; plane $x = 0$ at $y = 3, 4, 6, 9, 15$; plane $x = -2$ at $y = 0, 1, 2, 4, 6, 9, 15$. All electric wall potentials have been measured as potential difference of a needle against the reference potential.

In order to measure pressure differences in each duct five stainless steel tubes of 2 mm inner diameter have been welded on the duct centre line. The exact location of the taps is illustrated in figure 1.

The measurements of the wall potentials as well as the pressure difference measurements have been performed using the same procedure and the same facility as in the Z-bend experiment by Stieglitz *et al.* (1996). The correction which has to be made in the pressure measurements in strongly three-dimensional MHD-flows is documented in detail in that paper.

The experimentally obtained dimensionless data plotted in the figures below represent values which have an absolute error of less than 8 % using the Gaussian error propagation law. Plotted values for which an error exceeds this margin are indicated by error bars.

5. Equal flow rates (the mode $Q^{(i)} = \text{constant}$)

First, we present experimental results for $n = 1$, 3 and 5 for equal flow rates in all the bends (the mode $Q^{(i)} = \text{constant}$) and for $\Theta = \beta = 0°$. Variations from these conditions will be discussed in §§5.4, 6. According to the asymptotic model the complete solution is known once the potentials on the duct walls and the pressure are determined. Thus, presentation of the experimental data is restricted to these quantities at some characteristic positions, which are marked by thick lines in the graphs. Similar tendencies have been observed at the other positions.

5.1. *Single bend* ($n = 1$)

Figure 3 shows theoretical and experimental values of the wall potential for a fixed Hartmann number and for varying N in different planes $(x, y) = \text{constant}$. Pairs of ducts 2 and 3 are empty. As has been mentioned in §3, the walls of the empty ducts serve as additional electrical current paths. All the subgraphs show that the potential on the walls of the empty ducts is far from constant. Thus, quite significant amount of the electric current flows within the walls, affecting the pressure drop and the flow distribution in the filled duct.

https://doi.org/10.1017/S0022112097005788 Published online by Cambridge University Press

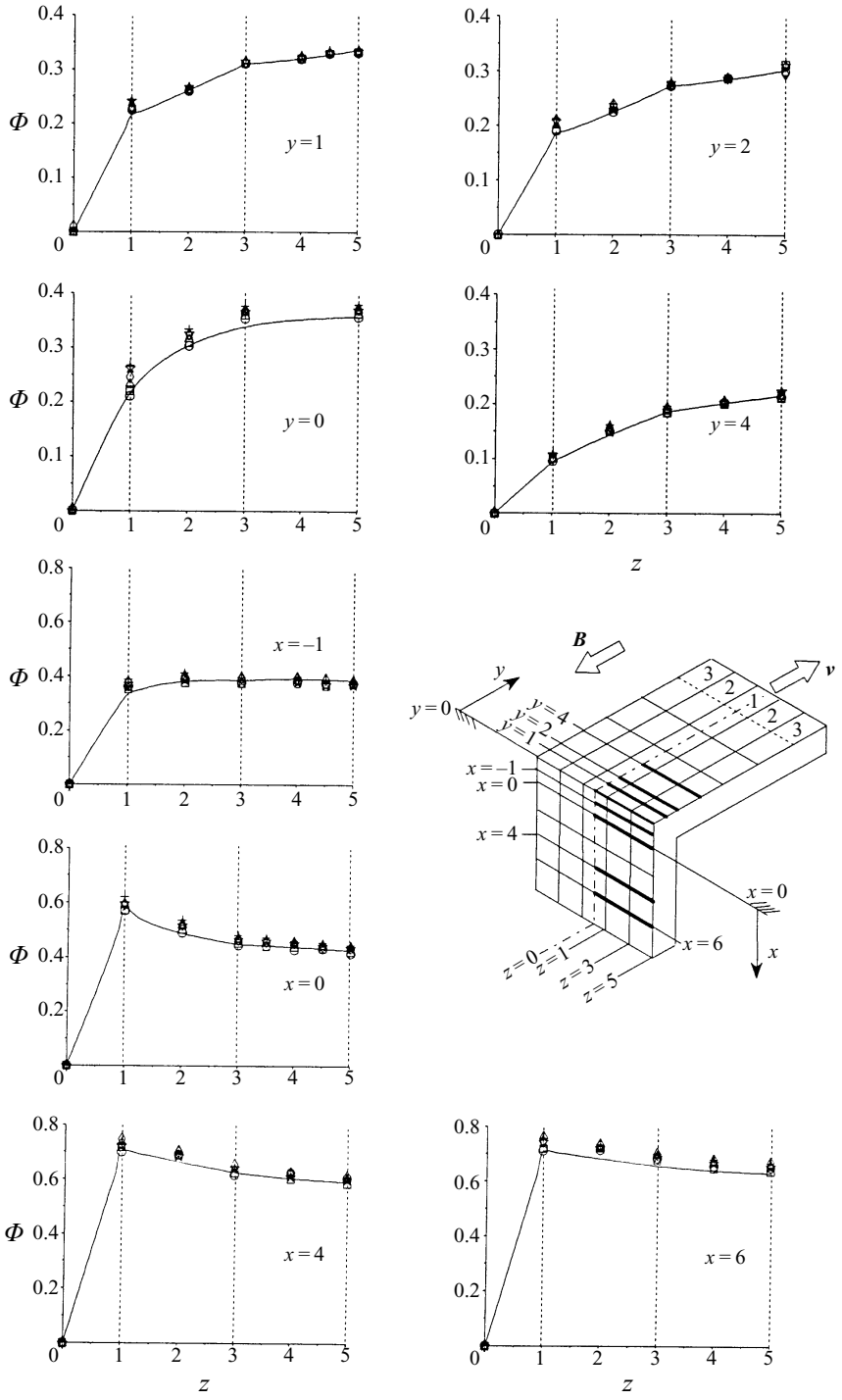


FIGURE 3. Wall potential distribuiton for $n = 1$; $M = 2365$; $c = 0.038$ and $\Theta = \beta = 0°$. ○, $N = 32390$; □, $N = 23900$; △, $N = 9436$; ◇, $N = 5778$; ☆, $N = 2004$; +, $N = 1101$; ——, calculation as N, $M \to \infty$.

https://doi.org/10.1017/S0022112097005788 Published online by Cambridge University Press

As the flow approaches the junction from $x = 6$ to $x = 0$ the value of the induced potential decreases continuously. The agreement between the calculated and the measured data there is rather good. The influence of the interaction parameter on the wall potentials is insignificant. In the immediate vicinity of the bend region, especially at the positions $x = -1$ and $y = 0$, slight discrepancies between the theory and the experiment occur. At $y = 0$, $z = 1$ near the sidewall of duct $i = 1$ a dependence of the wall potential on the interaction parameter is observed. As the flow passes the bend region the potential decreases further with increasing y-coordinate, and the agreement between the theory and the experiment becomes very good again. Similar conclusions have been made by Stieglitz *et al.* (1996), who investigated flow in a Z-bend.

5.2. *Three bends* ($n = 3$)

5.2.1. *Wall potential measurements*

The results for the wall potentials for different N and M are shown in figures 4 and 5. In figure 4 the wall potentials for different Hartmann numbers at a constant value of $N = 1034$ are shown for $n = 3$, $Q^{(i)} = \text{constant}$. At a distance of more than two values of the characteristic length away from the junction no influence of M is observed either on the Hartmann wall $y = 0$, nor on the wall $x = -2$. The recorded data practically coincide with the calculated ones. At the outer corner indicated as hatched area in figure 4, however, a certain dependence of the potential on M is found. With increasing M the experimental data have a tendency to approach those predicted by the asymptotic model. Nevertheless, the measured data in the middle of duct $i = 2$ (at $z = 2$) are significantly lower than the asymptotic ones not only at the outer corner but also at the junction $x = 0$. At that position for $z = 2$ the potential does not have the tendency to approach theoretical values for increasing M at all. In contrast, at the duct walls at $z = 1$ and $z = 3$ the calculated values are almost exactly confirmed by the measurement. A plot of the potential data at the position $x = -1$ versus $M^{-1/2}$, is shown in figure 6(*a*). Unfortunately, no definite conclusion can be made on the type of dependence on M of this quantity owing to the lack of data. However, the fact that there is a dependence of the potential on M on the Hartmann wall is shown for the first time for such high values of N and M, and is therefore surprising. In a single bend flow (§5.1) such a variation at the Hartmann wall has not been observed.

The potential distribution at several characteristic positions for the same flow configuration at a fixed Hartmann number of $M = 2431$ and different values of N is presented in figure 5. Again, at two values of the characteristic length away from the junction, i.e. for $x > 2$ and for $y > 2$, the measured potentials show no influence of N and, moreover, agree nearly exactly with the asymptotic values for an inertialess flow.

The results shown in figures 4 and 5 outline that the flow in the radial-duct cores of bends $i = 1$ and $i = 2$ at a few values of the characteristic length away from the bend is inviscid and inertialess in the parameter range investigated. But in the immediate vicinity of the bend a dependence of the potentials on N is observed. Figure 6(*b*) shows the wall potentials at the position $x = -1$, $y = 0$ versus $N^{-1/3}$. Again, no definite conclusion can be made about the dependence on N, although one might try to fit a straight line to approximate the measured values. The question whether the potential at this point varies linearly with $N^{-1/3}$ remains open.

The disagreement in the potentials between the model and the experiment at $z = 2$ in the toroidal duct $i = 2$ (e.g. at $x = -1$) for all experimental values of M and N leads to a different distribution of the core velocity in this duct. The lower z-derivative of the wall potential in the region $1 \leqslant z \leqslant 2$ compared to the model leads to a lower core

https://doi.org/10.1017/S0022112097005788 Published online by Cambridge University Press

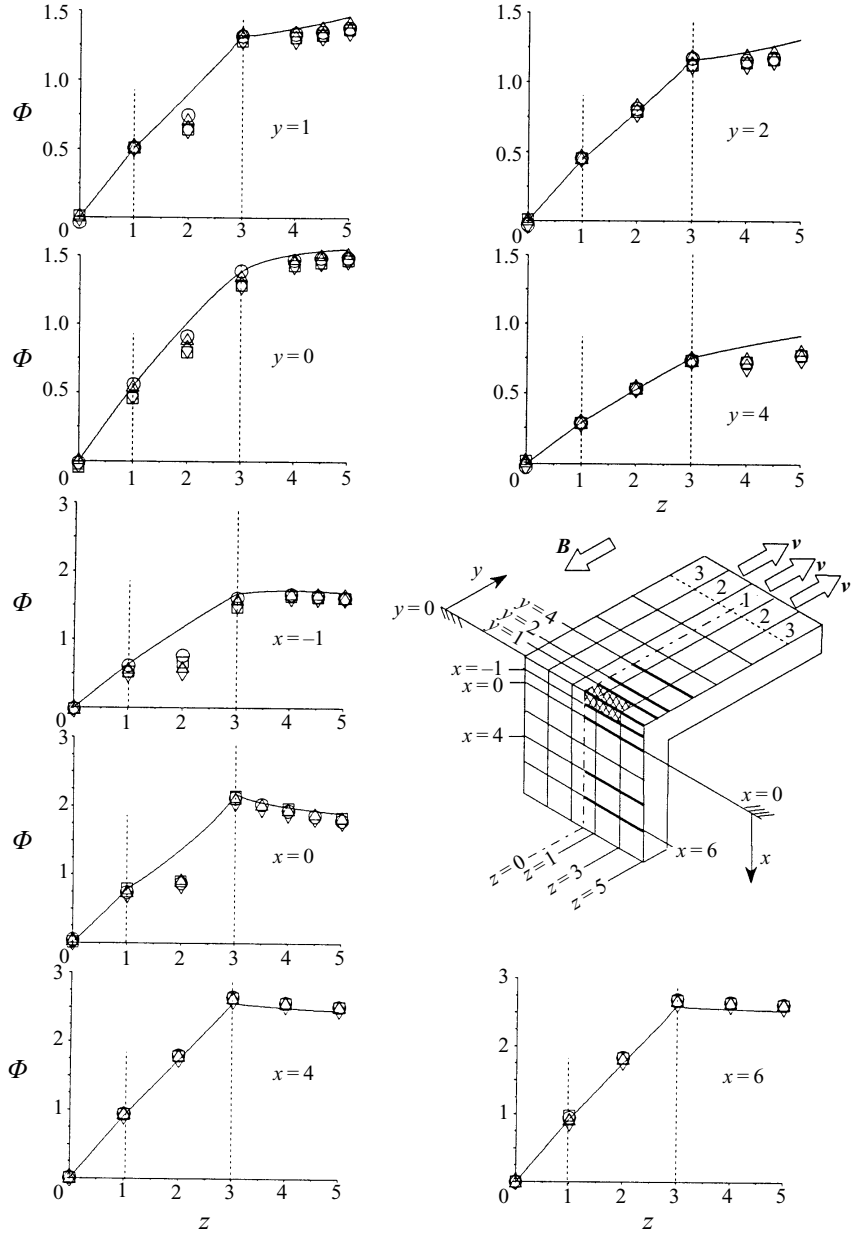


FIGURE 4. Wall potential distribution for $n = 3$; $Q^{(i)} = \text{constant}$; $N = 1034$; $c = 0.038$ and $\Theta = \beta = 0°$. ○, $M = 2431$; □, $M = 1910$; △, $M = 1211$; ◇, $M = 634$; ——, calculation as $N, M \to \infty$.

velocity in the x-direction, whereas the higher derivative in the domain $2 \leqslant z \leqslant 3$ indicates a higher core velocity than predicted by the model (cf. (3.5)). Of course, (3.5) is applicable as long as $|\boldsymbol{j} \times \hat{\boldsymbol{y}}| \ll 1$, which is fulfilled in the theory but might not be fulfilled in the experiment. The electric potential at the dividing wall $z = 3$ (but not at $z = 1$) coincides with the calculated one in the whole investigated parameter range. The potential distribution on the walls of the unfilled ducts agrees rather well in all domains with the values predicted by the asymptotic model and is independent of both the Hartmann number and the interaction parameter.

https://doi.org/10.1017/S0022112097005788 Published online by Cambridge University Press

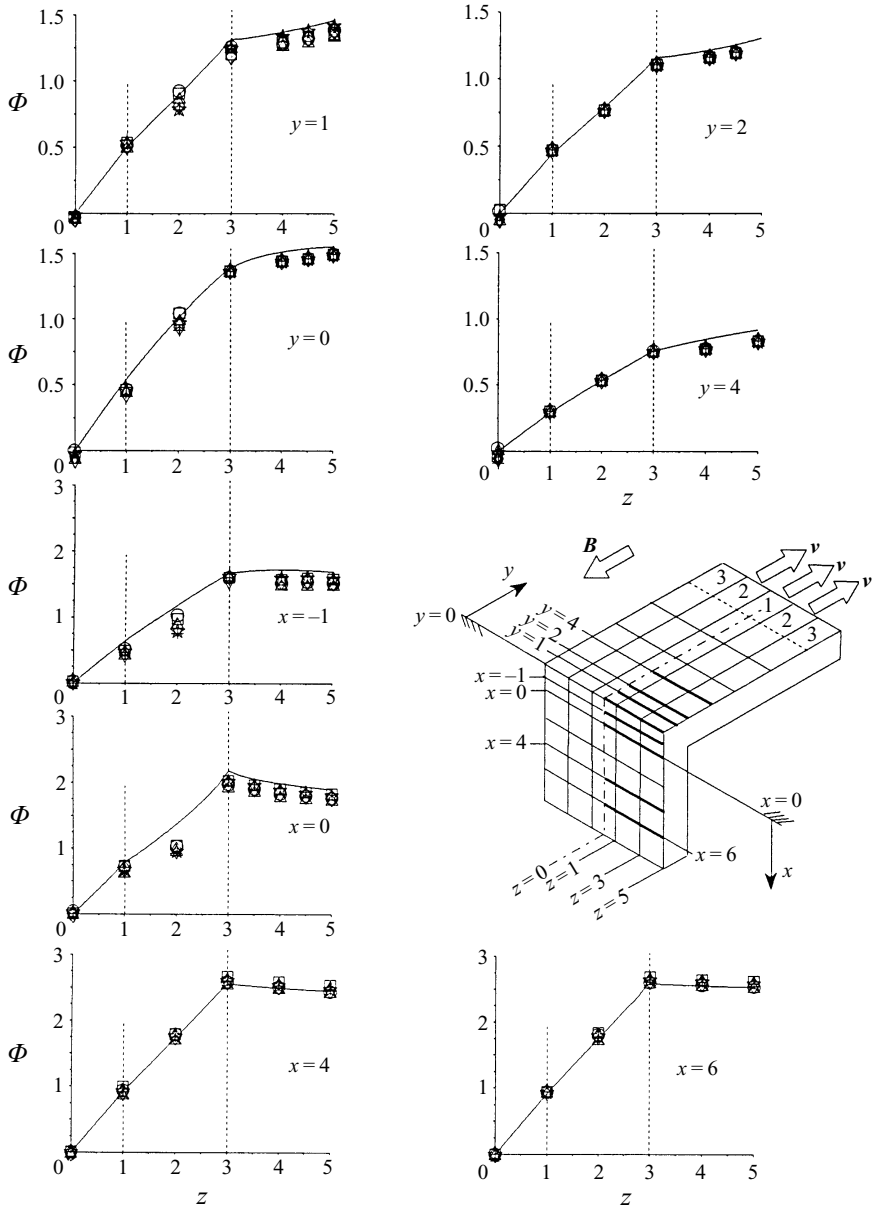


FIGURE 5. Wall potential distribution for $n = 3$, $Q^{(i)} = \text{constant}$; $M = 2431$; $c = 0.038$ and $\Theta = \beta = 0°$. ○, $N = 37436$; □, $N = 20355$; △, $N = 10457$; ◇, $N = 4153$; ☆, $N = 1827$; +, $N = 1034$; ——, calculation as $N, M \to \infty$.

5.2.2. *Pressure difference measurements*

The question of the pressure drop is very important. In order to separate different effects, the total pressure drop Δp_{total} between any two points along the duct can be split into several parts as follows:

$$\Delta p_{total} = \Delta p_{2D} + \Delta p_{3D,C} + \Delta p_{3D,N}(N) + \Delta p_{3D,M}(M). \tag{5.1}$$

The first part, the so-called two-dimensional pressure drop Δp_{2D} may be calculated using the asymptotic solution for the flow in a system of electrically coupled straight

https://doi.org/10.1017/S0022112097005788 Published online by Cambridge University Press

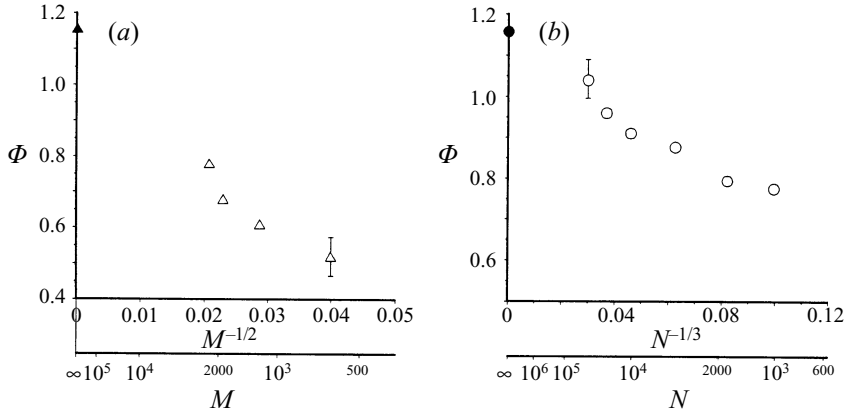


FIGURE 6. Measured Hartmann-wall potential at the point $x = -1$; $y = 0$ for $n = 3$, $Q^{(i)} = \text{constant}$; $\Theta = \beta = 0°$, $c = 0.038$. The filled symbols represent the values calculated for M, $N \to \infty$. (*a*) Potential for $N = 1034$ as a function of $M^{-1/2}$; (*b*) potential for $M = 2431$ as a function of $N^{-1/3}$.

$\Delta p_{total,\,i.2\text{–}i.5}$	$\Delta p_{2D} + \Delta p_{3D,\,C}$	$\Delta p_{3D,\,N}\ (N)$	$\Delta p_{3D,\,M}\ (M)$
Duct $i = 1$	0.57	$3.85 \times N^{-0.325}$	$1.2 \times M^{-0.475}$
Ducts $i = 2$	0.45	$2.34 \times N^{-0.320}$	$1.2 \times M^{-0.473}$

TABLE 1. Contributions of different parts of the pressure drop obtained with a fitting procedure for $n = 3$ with $Q^{(i)} = \text{constant}$; $c = 0.038$ and $\Theta = \beta = 0°$

ducts obtained by Molokov (1993). Δp_{2D} has to be taken into account in the radial ducts only, because in the toroidal ducts it vanishes to the main order (Molokov & Bühler 1994; Molokov & Stieglitz 1995). The other terms in (5.1) represent contributions to the so-called three-dimensional pressure drop Δp_{3D}, which expresses the excess pressure drop required for reshaping the velocity profile near the junction. In the asymptotic model in which only Lorentz and pressure forces act on the fluid a three-dimensional pressure drop $\Delta p_{3D,\,C}$ caused by Joulean dissipation of three-dimensional electric currents appears and can be calculated. The last two terms in (5.1) represent the contribution of parallel layers with electromagnetic–inertia and viscous–electromagnetic interaction. They can be determined up to now only experimentally. One should keep in mind that the attempt to express the pressure drop as formulated in (5.1) neglects viscous–inertia interaction, which is present in a real MHD flow.

A least-square fitting procedure for the measured data for both ducts $i = 1$ and $i = 2$ yields the results shown in table 1. The constants in column 2 for both $i = 1$ and $i = 2$ differ by about 10 % from the values calculated with the model. The exponents for N and M are nearly $-1/3$ for N and $-1/2$ for M, in complete agreement with the order-of-magnitude analysis by Hunt and Holroyd (1977) for bend flows. Similar exponents have been obtained in the Z-bend experiment by Stieglitz *et al.* (1996). The significance of this result for bend flows and for general three-dimensional magnetohydrodynamic flows has been discussed by Molokov *et al.* (1995) and Stieglitz *et al.* (1996).

In figure 7 the dimensionless pressure drop in a three-channel flow in the radial duct $i = 1$ between positions 1.1 and 1.2 is shown for $M = 2386$ as a function of $N^{-1/3}$. Both calculations and measurements indicate that the flow is far from fully developed in the

https://doi.org/10.1017/S0022112097005788 Published online by Cambridge University Press

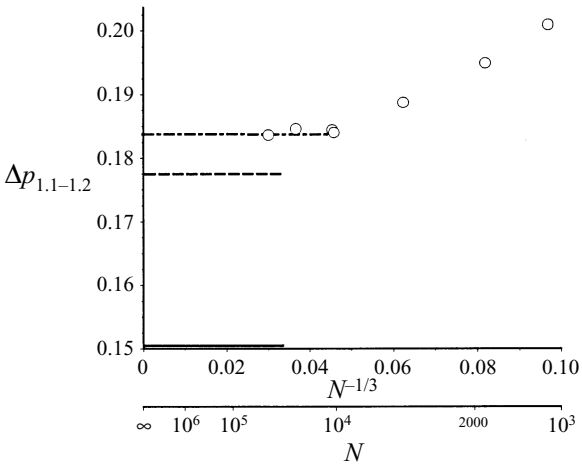


FIGURE 7. Pressure drop in the radial duct $i = 1$ between the positions 1.1 and 1.2 for $n = 3$, $Q^{(i)} =$ constant; $M = 2386$; $c = 0.038$ and $\Theta = \beta = 0°$. ○, Measurement; ——, fully developed 2D-calculation with $M = 2386$. 3D-calculation as $M, N \to \infty$ with (–·–·–·) and (——) without taking into account the electric wall conductivity of the two unfilled outer ducts.

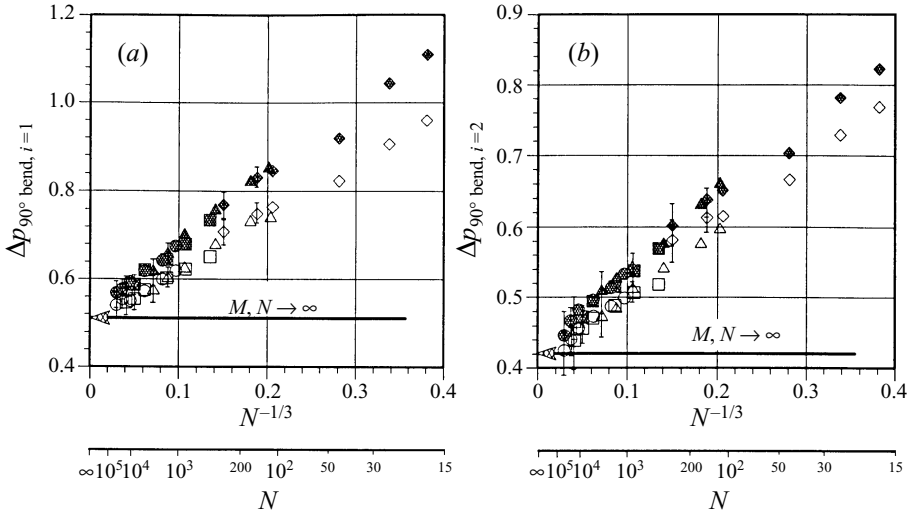


FIGURE 8. Measured pressure drop in the 90° bends for $n = 3$, $Q^{(i)} =$ constant; $c = 0.038$ and $\Theta = \beta = 0°$. ○, $M = 2386$; □, $M = 1796$; △, $M = 1205$; ◇, $M = 587$; ——, calculation as $M, N \to \infty$. The radial–toroidal flow measured between positions $i.2$ and $i.3$ is marked by open symbols; the toroidal–radial flow measured between positions $i.3$ and $i.5$ is indicated by the filled symbols. (*a*) Duct $i = 1$; (*b*) ducts $i = 2$.

whole test section. The data for Δp_{2D}, calculated with the code developed by Molokov (1993), are 16 % lower than the calculated pressure drop for the real U-bend geometry in the region between 1.1 and 1.2, where the fully developed flow was expected. A comparison of the experimental data for $N > 10^4$ with the value obtained by the asymptotic three-dimensional model demonstrates that with proper modelling quite a good agreement is achieved. However, for interaction parameters $N < 10^4$ a clear dependence of the pressure drop on inertia is observed.

In figure 8 the pressure drops between positions $i.2$ and $i.3$ (open symbols) and between positions $i.3$ and $i.5$ (filled symbols) are plotted both for duct $i = 1$ and the

https://doi.org/10.1017/S0022112097005788 Published online by Cambridge University Press

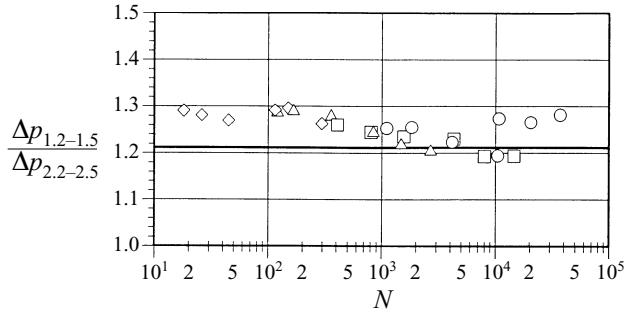


FIGURE 9. Ratio of the pressure drops in duct $i = 1$ and ducts $i = 2$ between positions $i.2$ and $i.5$ for $n = 3$, $Q^{(i)} = \text{constant}$; $c = 0.038$ and $\Theta = \beta = 0°$ as a function of N at different Hartmann numbers. ○, $M = 2386$; □, $M = 1796$; △, $M = 1205$; ◇, $M = 587$; ——, calculation as N, $M \to \infty$.

ducts $i = 2$ at different values of N in order to investigate the influence of the bend orientation (radial → toroidal flow or toroidal → radial flow in two 90°-bends comprising the U-bend). In both ducts 1 and 2 a difference between these two flow configurations has been found throughout the parameter range investigated. As in the Z-bend experiment by Stieglitz *et al.* (1996) the pressure drop in a toroidal → radial bend is higher than in a radial → toroidal bend. The reason for this difference arises from the development of separation areas beyond the corners. In a toroidal → radial flow the separation area may develop near the top Hartmann wall at $x > 0$, $y > 22$. Compared to the opposite flow direction it will be much shorter but it can be thicker. The induced potential in this separation area is lower. Therefore, the Ohmic resistance of the zone in the toroidal → radial flow is smaller, which leads to a higher current and thus to a higher pressure drop. For high N ($N > 10^4$) the pressure drop for both flow directions is nearly the same within the measurement accuracy. As M and N tend to infinity both in duct $i = 1$ and the ducts $i = 2$ the pressure drops tend to the values calculated by the asymptotic model.

Also, a dependence of the pressure drop on the Hartmann number is observed in the bend experiments: at the same value of the interaction parameter the dimensionless pressure drop increases with decreasing Hartmann number. Plotting the ratio of the total pressure drop in duct $i = 1$ and ducts $i = 2$ between positions $i.2$ and $i.5$ as a function of the interaction parameter and for different Hartmann numbers, one observes that this ratio is almost constant, see figure 9. The ratio depends neither on N nor on M and corresponds nearly to the value predicted by the asymptotic theory. Owing to the good agreement it can be concluded that the flow distribution between the core and the parallel layers is predicted correctly by the inertialess model and remains the same for all N and M in the parameter range investigated. This means that although the inertial parallel layers become thicker with decreasing N than the inertialess ones, the amount of flow carried by the jets in these layers remains the same or almost the same.

5.3 *Five bends* ($n = 5$)

5.3.1. *Wall potential measurements*

The potential distribution in a five-channel flow for different values of the interaction parameter is shown in figure 10. Analogously to the three-channel flow the agreement between the experiment and the asymptotic model at a distance of more than two values of the characteristic length away from the bend area is very good.

However, in the vicinity of the bend a drastic qualitative and quantitative disagreement between the model and the experiment appears, which is most apparent

https://doi.org/10.1017/S0022112097005788 Published online by Cambridge University Press

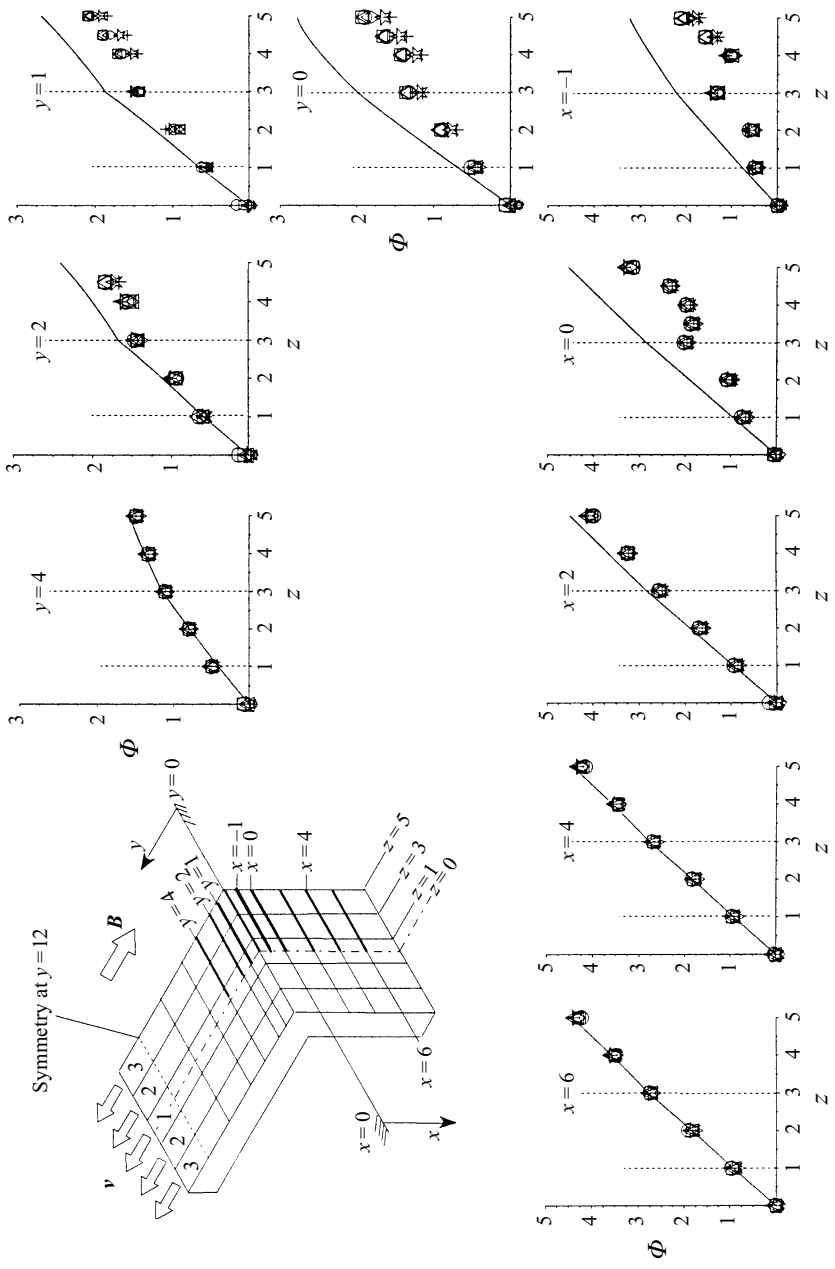


FIGURE 10. Wall potential distribution for $n = 5$, $Q^{(i)} = \text{constant}$; $M = 2431$; $c = 0.038$ and $\Theta = \beta = 0°$. ○, $N = 43388$; □, $N = 26327$; △, $N = 14784$; ◇, $N = 5590$; ☆, $N = 2350$; +, $N = 1292$; ——, calculation as N, $M \to \infty$.

https://doi.org/10.1017/S0022112097005788 Published online by Cambridge University Press

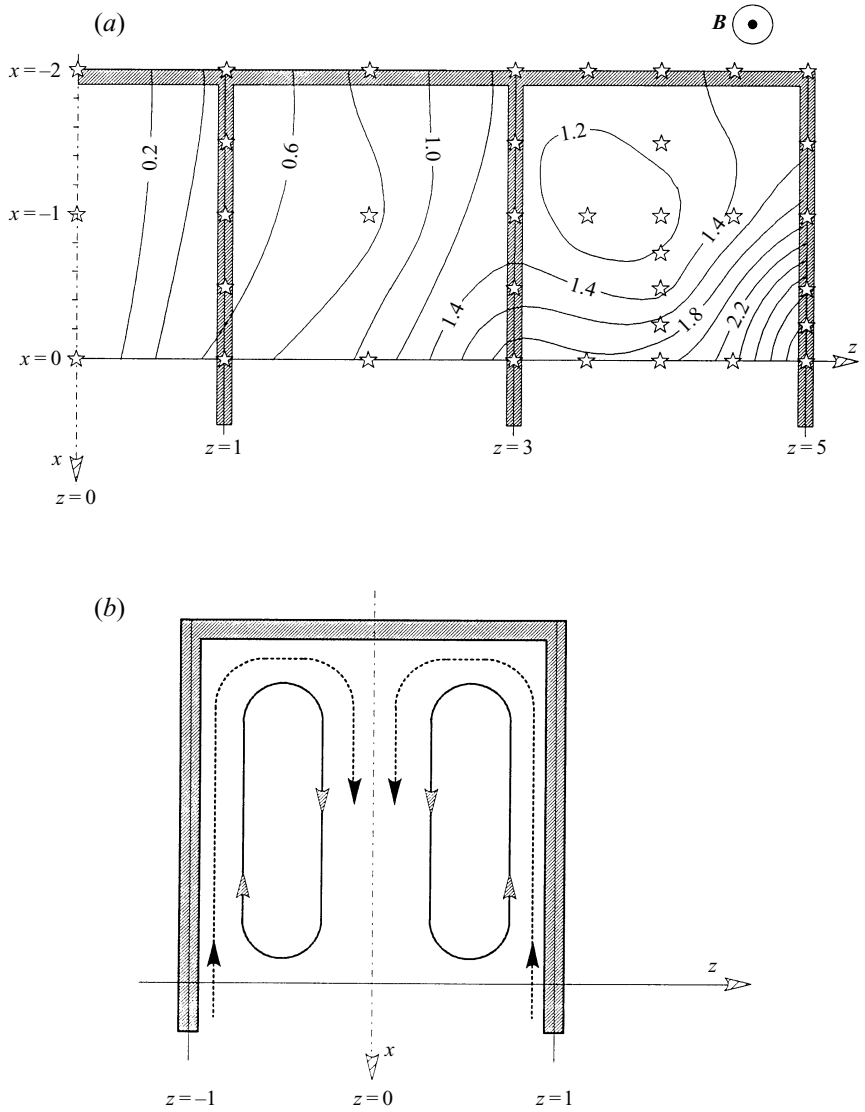


FIGURE 11. (*a*) Measured isopotential distribution at $y = 0$, $x < 0$ for $n = 5$, $Q^{(i)} = \text{constant}$, $N = 2350$; $M = 2431$; $c = 0.038$, and $\Theta = \beta = 0°$. The stars indicate the measurement points. (*b*) Sketch of flow pattern in the experiment by Reimann *et al.* (1995): jets bursting into the core (dotted lines); recirculating flow pattern in the core (solid lines).

in ducts $i = 2$ and $i = 3$. The measured potentials there are much lower than the calculated ones. The smaller potential gradient in the region $1 \leqslant z \leqslant 4$ for $x \leqslant 2$ may indicate that the core velocity there is smaller than that predicted by the model. But the potential gradient near the outer wall at $z \geqslant 4$ suggests a higher velocity. A significant influence of M and N on the potentials is found only in the toroidal part of bends $i = 3$ for $y \leqslant 2$.

In the following discussion we assume that by virtue of (3.5) the isolines of the electric potential at $y = 0$, $x < 0$ reflect the streamlines in the cores of the toroidal ducts not only in the theory, but also in the experiments. We recall that (3.5) is applicable as long as $|\boldsymbol{j} \times \hat{\boldsymbol{y}}| \ll 1$.

https://doi.org/10.1017/S0022112097005788 Published online by Cambridge University Press

In figure 11(*a*) the isopotential contour plot of the measured values in the toroidal ducts at $y = 0$ is shown. A comparison with the calculated isopotential distribution shown in figure 2 demonstrates the differences in the flow pattern establishing in an inertial MHD bend flow. In duct $i = 1$ ($z \leqslant 1$) the calculated potential distribution is similar to that found in the experiment. In ducts $i = 2$ and $i = 3$ the isopotential lines indicate that more fluid is pushed towards the outer sidewalls at $z = 3$ and $z = 5$ than calculated. Furthermore, the main feature depicted in the isolines in the ducts $i = 3$ is the appearance of a closed streamline on the (x, z)-plane.

A similar flow pattern in a single U-bend has been obtained experimentally by Reimann *et al.* (1995) in highly inertial flow conditions ($N \leqslant 150$, $M \leqslant 460$). In these experiments hot-wire anemometers and potential probes were inserted into the liquid metal. Although it is known that these probes affect the flow itself (see e.g. the discussion by Stieglitz *et al.* 1996), the results for the wall potential presented here confirm that, at least qualitatively, the results of Reimann *et al.* are correct.

The projection of the flow pattern on the (x, z)-plane in the experiments by Reimann *et al.* (1995) is sketched in figure 11(*b*), which shows that the y-component of vorticity has the opposite sign to that predicted theoretically (cf. figure 2, $i = 1$). This pattern extends into the major part of the toroidal duct and is claimed to be virtually two-dimensional along the magnetic field lines. This contrasts with the inertialess flow, where both x- and z-components of velocity vanish at the symmetry plane $y = l$. The explanation provided by Reimann *et al.* (1995) is the following. The jets at the sidewalls $z = \pm 1$ are characterized by a high momentum flux ρv^2. They penetrate into the toroidal duct and meet at the symmetry plane $z = 0$. In the inertialess flow the jets are turned in the y-direction by the electromagnetic forces, so that the jets decelerate smoothly towards $z = 0$. In the inertial flow for sufficiently low values of N, the momentum of the jets is not destroyed completely. When they meet at the symmetry plane $z = 0$, they burst in the x-direction into the core. As a result of this, the z-component of the gradient of the potential of the wall $y = 0$ changes the sign at $z = 0$, and closed isopotential lines appear as shown in figure 11(*b*). This distribution of potential drives a recirculatory flow in the core, provided the y-component of the core velocity is still zero. It should be noted that the latter is an assumption only, and the question of two-dimensionality of this flow pattern remains open.

A similar mechanism applies to the present flow, figure 11(*a*). In duct $i = 1$ the jets at the sidewalls are very weak (in theory they carry less than 1% of the total volume flux, see Molokov & Stieglitz 1995). They are much weaker than in a single bend, as in the experiments of Reimann *et al.* The reason for their weakness is that the amount of flow carried by a parallel layer at a sidewall is determined by the magnitude of current flowing in the plane of this wall (Molokov & Stieglitz 1995). In a single bend (experiments by Reimann *et al.*) all the fluid current enters the wall $z = 1$. In a multi-channel configuration most of the current induced in duct 1 crosses the wall $z = 1$ and enters duct 2, see figure 2. Only excess current flows in the wall in the $-x$-direction, leading to weak jets at $z = \pm 1$ that are unable to reverse potential gradient at $z = 0$ in the toroidal core.

In duct 2 the jet momentum at the sidewall $z = 3$ is higher than in duct 1, but still not sufficient to significantly affect the flow in the core.

In duct 3 a very strong jet enters the toroidal duct at the wall $z = 5$. Owing to its high momentum it reverses potential gradient at the wall $z = 3$, and produces a vortex pattern in the core of duct 3. As the number of bends increases this effect is expected to be more and more pronounced.

https://doi.org/10.1017/S0022112097005788 Published online by Cambridge University Press

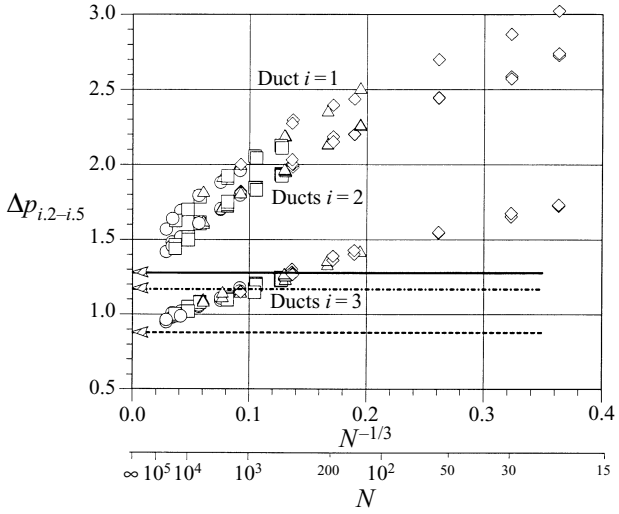


FIGURE 12. Measured pressure drop between positions $i.2$ and $i.5$ for $n = 5$, $Q^{(i)} = \text{constant}$; $c = 0.038$ and $\Theta = \beta = 0°$ as a function of $N^{-1/3}$ for different values of M: ○, $M = 2363$; □, $M = 1810$; △, $M = 1215$; ◇, $M = 607$. Calculations as N, $M \to \infty$: ———, duct $i = 1$; –·–·–·–, ducts $i = 2$; — — —, ducts $i = 3$.

$\Delta p_{total,\, i.2\text{–}i.5}$	$\Delta p_{2D} + \Delta p_{3D,\, C}$	$\Delta p_{3D,\, N}\ (N)$	$\Delta p_{3D,\, M}\ (M)$
Duct $i = 1$	1.33	$4.97 \times N^{-0.33}$	$1.16 \times M^{-0.507}$
Ducts $i = 2$	1.26	$3.90 \times N^{-0.33}$	$1.30 \times M^{-0.495}$
Ducts $i = 3$	0.88	$2.00 \times N^{-0.33}$	$1.00 \times M^{-0.495}$

TABLE 2. Contributions of different parts of the pressure drop obtained with a fitting procedure for $n = 5$ with $Q^{(i)} = \text{constant}$; $c = 0.038$ and $\Theta = \beta = 0°$

5.3.2. *Pressure difference measurements*

The pressure drop between $i.2$ and $i.5$ in a five-channel flow with identical flow rates in each duct is shown in figure 12 as a function of $N^{-1/3}$ for different Hartmann numbers. For high N the measured pressure drop in the outer duct ($i = 3$) tends to the value calculated by the model. On extrapolating the pressure drop in the inner ducts ($i = 1$ and $i = 2$) as $N \to \infty$ the calculated inertialess limit is not exactly reached. The reason for the small deviation between the asymptotic model and the measurement may be the inclined inlet, which is not taken into account in the modelling. A similar fitting procedure as carried out in §5.2.2 leads to the results shown in table 2. Here also the exponents obtained for N and M are nearly $-1/3$ and $-1/2$, respectively.

For engineering purposes the dependence of the pressure drop on the number of electrically coupled ducts is of major importance. In figure 13 the pressure drop in the central duct ($i = 1$) is plotted versus the number of electrically coupled bends for different values of the interaction parameter. By comparing the multi-channel results of calculation and measurement with the numerical results for a single U-bend flow of equivalent width and equivalent volumetric flow rate, it is seen that the pressure drops in the multi-channel system are significantly higher. The reason for this is that the dividing walls at $z = 1$ and $z = 3$ provide additional paths for the electric current, thus increasing its magnitude (Molokov & Stieglitz 1995).

https://doi.org/10.1017/S0022112097005788 Published online by Cambridge University Press

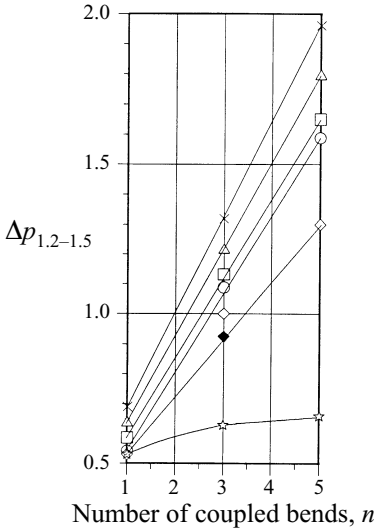


FIGURE 13. Measured pressure drop in duct $i = 1$ between positions 1.2 and 1.5 as a function of n for different values of N and for $Q^{(i)} = \text{constant}$; $c = 0.038$; $M = 2402$ and $\Theta = \beta = 0°$. ○, $N = 41410$; □, $N = 22077$; △, $N = 5154$; ×, $N = 1169$; ◇, calculation as N, $M \to \infty$; ◆, calculation for $n = 3$ not taking into account the unfilled neighbouring ducts; ☆, single bend ($n = 1$) with equivalent aspect ratio and equivalent volumetric flow rate.

Both in the measurements and the calculation the pressure drop increases in the central duct linearly with the number of electrically coupled bends. An upper limit of the pressure drop for increasing number of bends is not expected, as discussed by Molokov & Stieglitz (1995).

With increasing number of coupled ducts the inertial part of the pressure drop $\Delta p_{3D,\,N}$ also increases, which can be seen by the diverging lines for constant N in figure 13 as N decreases; it can reach the order of magnitude of the total inertialess pressure drop $\Delta p_{total} - \Delta p_{3D,\,N}$ calculated by the model.

5.4. *Influence of small B-field inclinations with respect to the* U*-bend*

For the design of heat transfer units it is of major importance to know how small magnetic field deviations from the perfectly aligned case influence the flow characteristics.

Because of the loss of symmetry by inclining the geometry with respect to $\boldsymbol{B}$, the code developed by Molokov & Stieglitz (1995) for $\Theta = \beta = 0°$ could not be applied to the inclined cases investigated. In the experimental results presented the differences to the aligned case are outlined.

5.4.1. *Inclination* $\Theta = 7°$, $\beta = 0°$

For an inclination of $\Theta \neq 0°$ the formerly aligned walls in the plane $x = 0$ and $x = -2$ become the Hartmann walls. The induced potential in the radial ducts varies to the first order as $\cos\Theta$ (cf. Moon & Walker 1990), whereas in the toroidal ducts it is proportional to $\sin\Theta$. The symmetry of the flow with respect to the plane $z = 0$ remains intact, but the symmetry about the plane $y = l$ is lost. Thus, one 90°-bend becomes a forward bend and the other one a backward bend, figure 14(*b*), according to the terminology of Moon & Walker (1990), and Moon *et al.* (1991). A detailed description of the flow patterns and pressure distributions establishing in forward and backward

https://doi.org/10.1017/S0022112097005788 Published online by Cambridge University Press

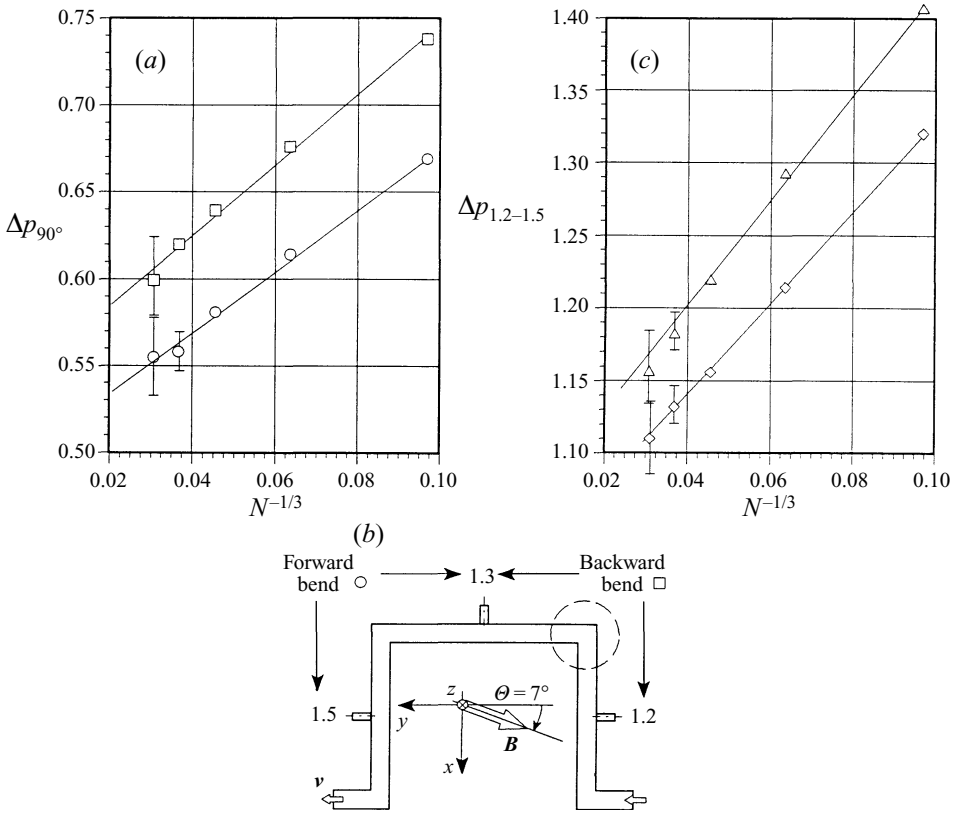


FIGURE 14. Pressure drop in the central bend $i = 1$ for $n = 3$, $Q^{(i)} =$ constant; $c = 0.038$ and $\Theta = 7°$, $\beta = 0°$ as a function of $N^{-1/3}$. (*a*) $\Theta = 7°$: □, backward bend; ○, forward bend. (*b*) Side view of the test section and definition of a forward and a backward bend. (*c*) Comparison of the total pressure drop between positions 1.2 and 1.5 for $\Theta = 7°$ (△) and $\Theta = 0°$ (◇).

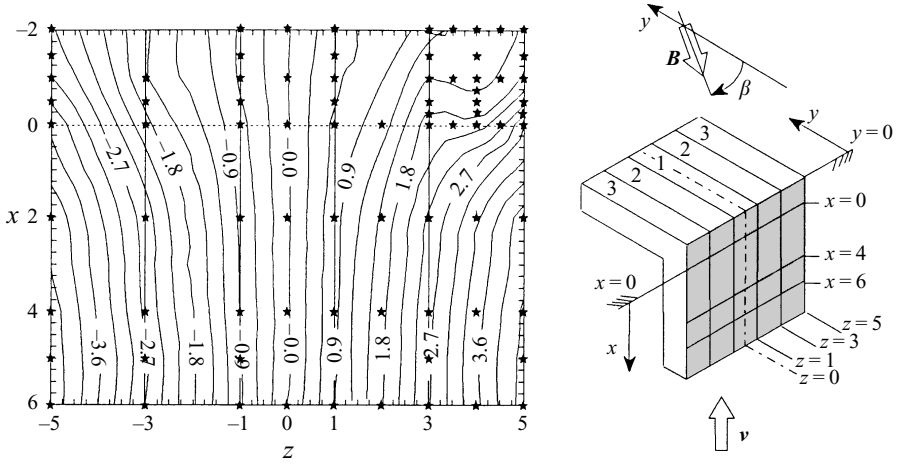


FIGURE 15. Isopotential distribution on the wall $y = 0$ for $n = 5$, $Q^{(i)} =$ constant; $c = 0.038$; $M = 2417$; $N = 17688$; $\Theta = 0°$ and $\beta = 9°$. ★, Measurement positions.

https://doi.org/10.1017/S0022112097005788 Published online by Cambridge University Press

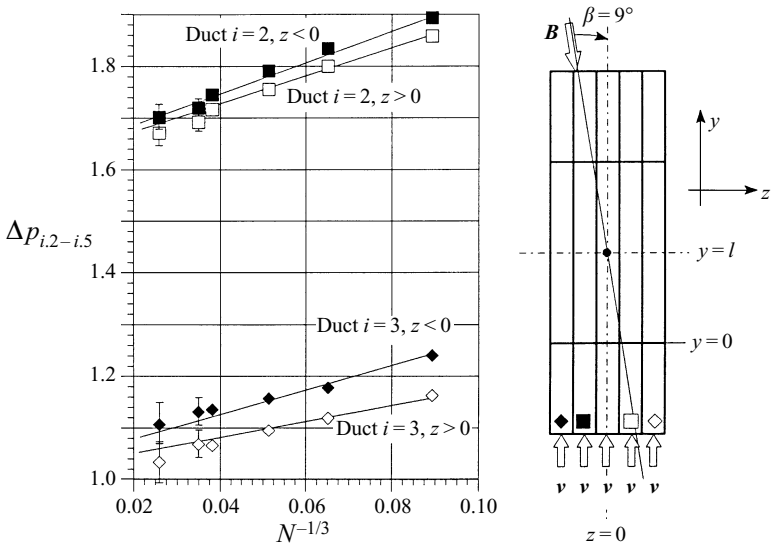


FIGURE 16. Measured pressure drop between positions $i.2$ and $i.5$ in the bends $i=2$ and $i=3$ for $n=5$, $Q^{(i)}=$ constant; $c=0.038$; $M=2417$; $\Theta=0°$ and $\beta=9°$ as a function of $N^{-1/3}$. The filled symbols indicate ducts with $z<0$, the open symbols mark ducts with $z>0$.

bends may be found in Moon & Walker (1990), Moon *et al.* (1991) and Stieglitz *et al.* (1996).

Because of the limited size of the magnet, only an inclination of $\Theta=7°$ has been investigated. Owing to the small inclination angle the induced potential changes only slightly in both the radial and the toroidal ducts. Variations of wall potentials with N and M are found to be almost the same as for the aligned case ($\Theta=0°$).

Figure 14(a) shows the pressure drop in the forward and backward bends of duct $i=1$ for $n=3$ with $Q^{(i)}=$ constant as a function of $N^{-1/3}$. Similarly to the experimental results for a flow in the Z-bend presented by Stieglitz *et al.* (1996), the pressure drop in a backward bend is higher than in a forward bend. The results reveal further that in both cases the inertial part of the pressure drop scales with $N^{-1/3}$. The influence of inertia on the pressure drop is stronger in the backward bend than the forward bend, which is documented in a higher slope of the fitted straight line.

In figure 14(c) the pressure drop in duct $i=1$ between positions 1.2 and 1.5 of the same flow is compared with the measured values for the inclination $\Theta=0°$. For the inclined configuration a higher pressure drop is found than for the aligned case ($\Theta=0°$). Moreover, the inertial part of the pressure drop increases more rapidly with decreasing N in the inclined case than in the aligned case. However, in both configurations it scales with $N^{-1/3}$.

5.4.2. *Inclination* $\beta=9°$, $\Theta=0°$

If the U-bend is inclined in the (y,z)-plane by an angle β, the flow loses its symmetry with respect to both planes $z=0$ and $y=l$. The sidewalls of the radial ducts as well as the sidewalls of the toroidal duct become the Hartmann walls.

Owing to the loss of symmetry with respect to the plane $z=0$ the potential distribution in the ducts $z>0$ is different than in the ducts $z<0$. In figure 15 the isopotential distribution in the plane $y=0$ of a five-channel flow with $\beta=9°$ is shown. As the flow approaches the junction at $x=0$ the asymmetry of the potentials with

https://doi.org/10.1017/S0022112097005788 Published online by Cambridge University Press

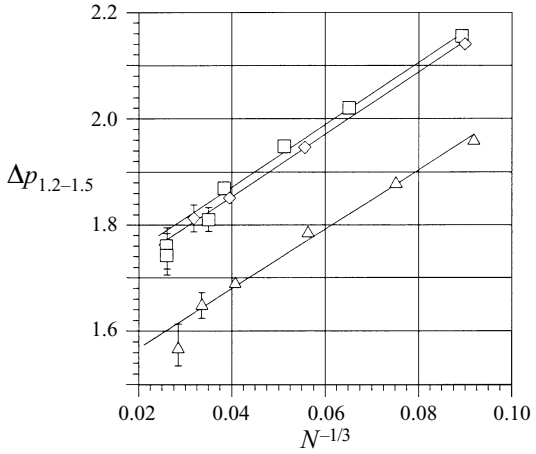


FIGURE 17. Comparison of the pressure drop in bend $i = 1$ between the positions 1.2 and 1.5 for $n = 5$, $Q^{(i)} = \text{constant}$; $c = 0.038$ and $M \approx 2400$ as a function of $N^{-1/3}$. $\triangle$, $\Theta = \beta = 0°$; $\diamond$, $\Theta = 7°$, $\beta = 0°$; $\square$, $\Theta = 0°$, $\beta = 9°$.

respect to $z = 0$ becomes stronger. The most significant differences in the wall potential compared to the case $\beta = \Theta = 0°$ are found in the outer ducts $i = 3$ between $x = 0$ and $x = -2$. The asymmetry in the potential distribution leads to changed current paths compared to the case $\beta = \Theta = 0°$, and therefore to uneven pressure drops in the individual ducts of the bends $y < l$. In the bend $y > l$ this uneven pressure distribution is reversed, so that if an inertialess flow is assumed, both effects should cancel.

In figure 16 the pressure drop in ducts $i = 2$ and $i = 3$ between positions $i.2$ and $i.5$ for $n = 5$ is shown as a function of $N^{-1/3}$. As N tends to infinity, i.e. $N^{-1/3} \to 0$, the extrapolations of the measured pressure drop lines nearly coincide for ducts $i = 2$ as well as for ducts $i = 3$. However, for $N > 5 \times 10^4$ the differences in the pressure drop between the ducts $z < 0$ and $z > 0$ are evident, which increase as $N^{-1/3}$ increases.

Figure 17 shows the pressure drop between 1.2 and 1.5 in the central duct $i = 1$ for $n = 5$ for the three investigated field inclination angles (i) $\Theta = \beta = 0°$, (ii) $\Theta = 7°$, $\beta = 0°$, and (iii) $\beta = 9°$, $\Theta = 0°$. The lowest pressure drop appears in the perfectly aligned case. However, this figure demonstrates that small field inclinations do not lead to a drastic pressure drop increase; the latter does not exceed 10 % in the investigated parameter range.

6. The mode $\Delta p^{(i)}$ constant

Another important flow mode, which we designate $\Delta p^{(i)} = \text{constant}$, occurs when the pressure drop in each sub-channel i between positions $i.2$ and $i.5$ is kept identical by adjusting the flow rates in each duct in an appropriate way. Some differences between the modes $Q^{(i)} = \text{constant}$ and $\Delta p^{(i)} = \text{constant}$ exist regarding both the flow distribution and the pressure drop.

Consider the flow in a three-channel bend ($n = 3$) with $\Delta p^{(i)} = \text{constant}$. In contrast to the mode $Q^{(i)} = \text{constant}$, the flow distribution between the bends becomes non-equal. The flow rate in the central duct $i = 1$ decreases, while that in ducts $i = 2$ increases (Molokov & Stieglitz 1995; Molokov 1993). The experiments show, however, that the ratio of the flow rates $Q^{(2)}$ and $Q^{(1)}$ is 1.58, and remains virtually the same throughout the parameter range investigated ($M = 6.2 \times 10^2$–2.3×10^3, $N =$

https://doi.org/10.1017/S0022112097005788 Published online by Cambridge University Press

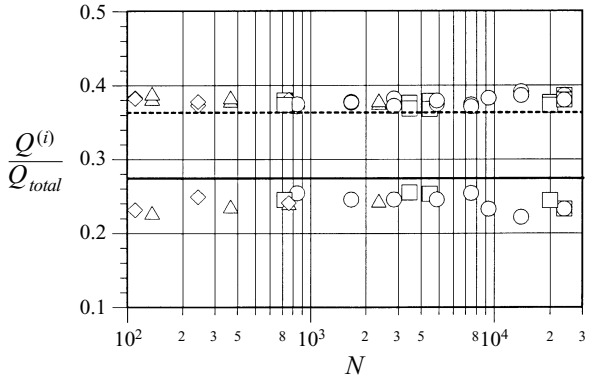


FIGURE 18. Measured flow rate ratio of duct $i = 1$ and ducts $i = 2$ to the total flow rate for $n = 3$, $\Delta p^{(i)} = \text{constant}$; $c = 0.038$; $\Theta = \beta = 0°$. ○, $M = 2363$; □, $M = 1810$; △, $M = 1215$; ◇, $M = 607$. Calculations as N, $M \to \infty$: duct $i = 1$ (solid line), and ducts $i = 2$ (dashed line).

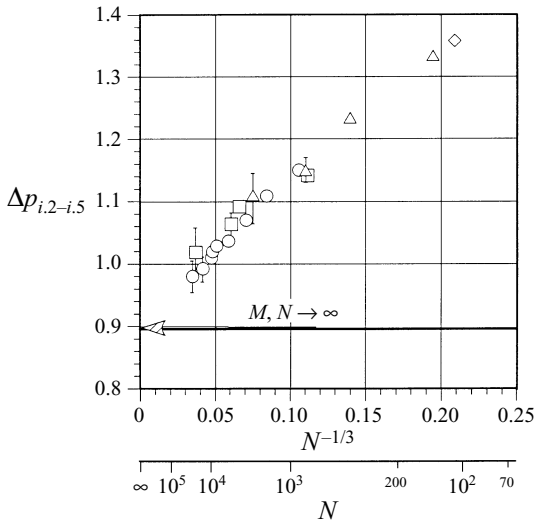


FIGURE 19. Measured pressure drop $\Delta p^{(i)}$ between the positions $i.2$ and $i.5$ for $n = 3$, $\Delta p^{(i)} = \text{constant}$; $c = 0.038$; $\Theta = \beta = 0°$. ○, $M = 2363$; □, $M = 1810$; △, $M = 1215$; ◇, $M = 607$, ——, calculation as M, $N \to \infty$.

1.1×10^2–2.6×10^4) (figure 18). It coincides with the calculated value for the inertialess flow. An important implication of this result is that the jets in the layers governed by the electromagnetic–inertia interaction carry the same volume flux as their inertialess counterparts (see also §5.2.2).

In contrast to the flow rates, the pressure drop $\Delta p^{(i)}$ exhibits a significant dependence on N as $N^{-1/3}$ (figure 19). As $N^{-1/3} \to 0$, the extrapolation of the experimental data reaches nearly the value predicted by the asymptotic model.

A comparison between the multi-channel U-bend flow in the mode $Q^{(i)} = \text{constant}$ with that in the mode $\Delta p^{(i)} = \text{constant}$ and with a single-bend flow (theoretical result) of the equivalent width and equivalent mean velocity is shown in figure 20, which demonstrates that the highest pressure drop is obtained for the mode $Q^{(i)} = \text{constant}$ for all values of M and N.

https://doi.org/10.1017/S0022112097005788 Published online by Cambridge University Press

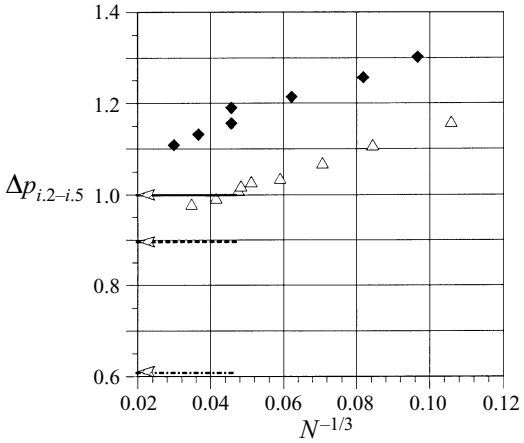


FIGURE 20. Comparison of the measured pressure drop in duct $i = 1$ between positions 1.2 and 1.5 for $n = 3$, $\Delta p^{(i)} =$ constant (open symbols) and $Q^{(i)} =$ constant (filled symbols) as a function of N for $M \approx 2400$; $c = 0.038$; $\Theta = \beta = 0°$. Calculations as M, $N \to \infty$ for $Q^{(i)} =$ constant (◁———) and for $\Delta p^{(i)} =$ constant (◁———) compared with a calculation for a single U-bend of equivalent width (◁–·–·–).

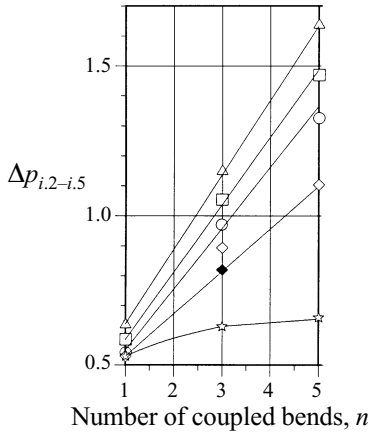


FIGURE 21. Pressure drop $\Delta p^{(i)}$ between positions $i.2$ and $i.5$ as a function of the number of electrically coupled bends for different N and for $\Delta p^{(i)} =$ constant, $c = 0.038$; $M = 2402$ and $\Theta = \beta = 0°$. ○, $N = 23458$; □, $N = 4861$; △, $N = 958$; ◇, Calculation as M, $N \to \infty$; ◆, calculation for $n = 3$, in which the non-filled neighbouring ducts are not taken into account; ☆, single duct with equivalent aspect ratio and equivalent volumetric flow rate.

In figure 21 the pressure drop between positions $i.2$ and $i.5$ is shown as a function of the number of electrically coupled ducts for different N in the mode $\Delta p^{(i)} =$ constant. Similarly to the mode $Q^{(i)} =$ constant the pressure drop increases linearly with the number of coupled bends; the slope of the lines, however, is lower.

The results for the wall potentials are qualitatively the same as for the mode $Q^{(i)} =$ constant; therefore, we do not discuss these results in more detail.

7. Conclusions

The experimental data for the pressure and the wall potentials show that in electrically coupled U-bends significant deviations between the inertialess asymptotic flow model and the measured data may occur. These deviations are not new in MHD

https://doi.org/10.1017/S0022112097005788 Published online by Cambridge University Press

(see e.g. the discussion by Holroyd 1980 and references therein). What is surprising is that they exist in very strong magnetic fields, which must have an impact on further development of strong-field magnetohydrodynamics.

In a single U-bend the agreement between the theory, valid for high M and very high N, and the experiment regarding the surface potentials is quite good. A weak dependence of the wall potential on N is found only in the immediate vicinity of the bends.

As the number of electrically coupled ducts increases to 3 and then to 5 a good agreement between the measurement and the model in the wall potentials is also found in the radial and the toroidal ducts except for the bend region. There first quantitative (for $n = 3$) and then qualitative (for $n = 5$) differences occur. The results for the wall potential provide strong evidence that in this region a completely different flow pattern is established compared to the one predicted by the asymptotic model. The potential measurements showed that in the five-channel configuration a recirculating flow appears directly in the bend region. In this region a weak dependence of the wall potential on M and N is found. Both dependencies indicate that a non-negligible current flow is carried by viscous and inertial boundary layers, modifying the current pattern and thus having a feedback on the pressure drop. With increasing Hartmann number and interaction parameter the measured data tend towards the theoretical values everywhere except for the bend region.

In both modes $\Delta p^{(i)} = \text{constant}$ and $Q^{(i)} = \text{constant}$ an increasing number of bends leads to a linear increase of the pressure drop in the central duct ($i = 1$). Moreover, the inertial part of the pressure drop grows with n. This linear increase of pressure drop in the central duct, which is amplified by the inertial effects, may be critical to the feasibility of multi-channel heat transfer units in fusion blanket applications, if an inadequate electrical separation is used or the insulation resistance fails due to irradiation or corrosion. Generally, the pressure drop for the mode most desirable in heat transfer units, namely $Q^{(i)} = \text{constant}$, is higher than for the mode $\Delta p^{(i)} = \text{constant}$.

The inertial part of the pressure drop in each flow configuration ($\Delta p^{(i)} = \text{constant}$; $Q^{(i)} = \text{constant}$) is proportional to $N^{-1/3}$. This scaling law is independent of the number of electrically coupled ducts and holds for each duct within the parameter range investigated. Moreover, the same dependence has been discovered in the Z-bend experiment (Stieglitz *et al.* 1996). The $N^{-1/3}$-variation of the pressure drop has been predicted for general three-dimensional flows in rectangular ducts by Hunt & Holroyd (1977). Now there is sufficient experimental evidence to conclude that their prediction was correct, so that in a very wide range of parameter variation the flow is governed by electromagnetic–inertia interaction in the layers parallel to the magnetic field. This balance of forces is different from the viscous–electromagnetic balance in inertialess flows, and the pressure differences measured in the U-bend for each flow configuration show that even for $N \approx 5 \times 10^4$ and $M \approx 2.4 \times 10^3$ the flow is far from being inertialess in the bend region. Therefore, the next stage in understanding of three-dimensional MHD flows in complex geometries can be achieved by developing a theory of nonlinear electromagnetic–inertia interaction.

This work has been carried out as part of Mr Stieglitz's PhD research at the Forschungszentrum Karlsruhe. There, this work has been performed in the framework of the Nuclear fusion project of the Forschungszentrum Karlsruhe and is supported by the European Union within the European Fusion Technology Program. The authors are grateful to Dr L. Barleon, Professor Dr -Ing, U. Müller, Dr J. Reimann, Dr L.

https://doi.org/10.1017/S0022112097005788 Published online by Cambridge University Press

Bühler and Mr K.-J. Mack from the Forschungszentrum Karlsruhe for their help in planning and performing the experiments and many hours of constructive discussions interpreting the experimental results.

REFERENCES

Barleon, L., Bühler, L., Mack, K.-J., Stieglitz, R., Picologlou, B. F., Hua, T. Q. & Reed, C. B. 1993 Liquid metal flow through a right angle bend in a strong magnetic field. *Fusion Technol.* **21**, 2197–2203.

Barleon, L., Bühler, L., Molokov, S., Stieglitz, R., Picologlou, B. F., Hua, T. Q. & Reed, C. B. 1994 Magnetohydrodynamic flow through a right angle bend. *Magnetohydrodynamics* **30**, 428–438.

Barleon, L., Casal, V. & Lenhart, L. 1991 MHD-flow in liquid metal cooled blankets. *Fusion Engng Design* **14**, 401–412.

Bühler, L. 1993 Magnetohydrodynamische Strömungen flüssiger Metalle in allgemeinen dreidimensionalen Geometrien unter der Einwirkung starker, lokal variabler Magnetfelder (in German). *Rep. KfK* 5095. Kernforschungszentrum Karlsruhe.

Bühler, L. 1995 Magnetohydrodynamic flows in arbitrary geometries in strong non-uniform magnetic fields – a numerical code for the design of fusion reactor blankets. *Fusion Technol.* **27**, 3–24.

Bühler, L. & Molokov, S. 1994 Magnetohydrodynamic flows in ducts with insulating coatings. *Magnetohydrodynamics* **30**, 439–447.

Holroyd, R. J. 1980 An experimental study of the effects of wall conductivity, non-uniform magnetic fields and variable-ara ducts on liquid-metal flows at high Hartmann number. Part 2. Ducts with conducting walls. *J. Fluid Mech.* **96**, 355–374.

Hua, T. Q. & Picologlou, B. F. 1991 Magnetohydrodynamic flow in a manifold and multiple rectangular coolant ducts of self-cooled blankets. *Fusion Technol.* **19**, 102–112.

Hua, T. Q. & Walker, J. S. 1991 MHD considerations for poloidal-toroidal coolant ducts of self-cooled blankets. *Fusion Technol.* **19**, 951–960.

Hunt, J. C. R. 1965 Magnetohydrodynamic flow in rectangular ducts. *J. Fluid Mech.* **21**, 577–590.

Hunt, J. C. R. & Holroyd, R. J. 1977 Applications of laboratory and theoretical MHD duct flow studies in fusion reactor technology. *UKEA-CLM-R-169*. Culham Laboratory, Abingdon, Oxfordshire, UK.

Hunt, J. C. R. & Leibovich, S. 1967 Magnetohydrodynamic duct flow in channels of variable cross-section with strong transverse magnetic field. *J. Fluid Mech.* **28**, 241–260.

Malang, S., Arheidt, K., Barleon, L., Borgstedt, H.-U., Casal, V., Fischer, U., Link, W., Reimann, J. & Rust, K. 1988 Self-cooled liquid-metal blanket concept. *Fusion Technol.* **14**, 1343–1356.

Molokov, S. 1993 Fully developed liquid-metal flow in multiple rectangular ducts in a strong uniform magnetic field. *Eur. J. Mech.* B *Fluids* **12**, 769–787.

Molokov, S. & Bühler, L. 1994 Liquid metal flow in a U-bend in a strong uniform magnetic field. *J. Fluid Mech.* **267**, 325–352.

Molokov, S. & Bühler, L. 1995 Asymptotic analysis of magnetohydrodynamic flows in bends. *Z. Angew. Math. Mech.* **75S**, 345–346.

Molokov, S., Bühler, L. & Stieglitz, R. 1995 Asymptotic structure of magnetohydrodynamic flows in bends. *Magnetohydrodynamics* **31**, 357–365.

Molokov, S. & Stieglitz, R. 1995 Liquid metal flow in a system of U-bends in a strong uniform magnetic field. *J. Fluid Mech.* **299**, 73–95.

Moon, T. J., Hua, T. Q. & Walker, J. S. 1991 Liquid metal flow in a backward elbow in the plane of a strong magnetic field. *J. Fluid Mech.* **227**, 273–292.

Moon, T. J. & Walker, J. S. 1990 Liquid metal flow through a sharp elbow in the plane of a strong magnetic field. *J. Fluid Mech.* **213**, 397–418.

O'Donell, J. O., Papanikolaou, P. G. & Reed, C. B. 1989 The thermophysical transport properties of eutectic NaK near room temperature. *Argonne National Laboratory – Fusion Power Program TM*-237.

https://doi.org/10.1017/S0022112097005788 Published online by Cambridge University Press

Reed, C. B., Picologlou, B. F., Hua, T. Q. & Walker, J. S. 1987 ALEX results – a comparison of measurements from a round and a rectangular duct with 3-D code predictions. *IEEE* 87CH2507-2 **2**, 1267.

Reimann, J., Bucenieks, I., Dementiev, S., Flerov, A., Molokov, S. & Platnieks, I. 1995 MHD-velocity distributions in U-bends partially parallel to the magnetic field. *Magnetohydrodynamics* **31**, 338–348.

Reimann, J., Molokov, S., Platnieks, I. & Platacis, E. 1993 MHD-flow in Multichannel U-bends: Screening tests and theoretical analysis. *Rep. KfK* 5102. Kernforschungszentrum, Karlsruhe.

Stieglitz, R. 1994 Magnetohydrodynamische Strömungen in Ein- und Mehrkanal-umlenkungen. PhD thesis, University of Karlsruhe (in German).

Stieglitz, R., Barleon, L., Bühler, L. & Molokov, S. 1996 Magnetohydrodynamic flow in a right angle bend in a strong magnetic field. *J. Fluid Mech.* **326**, 91–123.

Stieglitz, R., Molokov, S., Barleon, L., Reimann, J. & Mack, K.-J. 1994 MHD-flows in electrically coupled bends. Proc. 2nd Intl Conf. on Energy Transfer in Magnetohydrodynamic Flows, *Aussois*, *France*, *26th–30th Sept. 1994*, vol. 1, pp. 403–412.

Walker, J. S. 1981 Magnetohydrodynamic flows in rectangular ducts with thin conducting walls. Part I. *J. Méc.* **20**, 79–112.

https://doi.org/10.1017/S0022112097005788 Published online by Cambridge University Press